Sub-scale ballistic testing of an ultrafine grained tungsten alloy into concrete targets

Sub-Scale Ballistic Testing of an Ultrafine Grained Tungsten Alloy into Concrete Targets

Authors: Zachary C. Cordero[1], Ryan R. Carpenter[2], Christopher A. Schuh[1], Brian E. Schuster[3]

1. Department of Materials Science and Engineering, MIT, Cambridge MA 02139
2. US Army Armament Research Development Engineering Center, Picatinny Arsenal, NJ 07806
3. Weapons and Materials Research Directorate, Army Research Laboratory, Aberdeen Proving Ground MD 21005

Abstract:

Ultrafine grained tungsten-based alloys are promising kinetic energy penetrator materials because of their high strengths and densities, making them ideal for penetration into concrete and geomaterials. However, there are difficulties in evaluating their ballistic performance using traditional testing techniques because ultrafine grain sizes are challenging to achieve in bulk parts. In this letter, we performed sub-scale ballistic experiments where ultrafine tungsten alloy cores were fired into concrete targets using small caliber projectile assemblies. The results suggest that sub-scale testing may be used as a screening tool for advanced kinetic energy penetrator materials that are more easily prepared in smaller geometries.

Keywords: ultrafine grain, tungsten, rigid body penetration

1. Introduction

High-density alloys with ultrafine and nanocrystalline grain sizes possess a unique set of mechanical properties that make them very attractive kinetic energy penetrator materials for rigid body penetration into concrete and geomaterials. Their high strengths, for instance, suggest that they should remain elastic at incident velocities where penetrators made from softer materials, e.g., high strength steels, start to deform plastically [1–3].

Despite such promising properties, there have been few experimental studies evaluating the ballistic performance of these ultrafine grain penetrator materials. One reason for this is that many of the standard protocols for characterizing penetration performance call for penetrators with

dimensions that are difficult to achieve in parts with ultrafine grain sizes. For example, the Forrestal framework for evaluating the performance of rigid body penetrators into concrete was originally developed for penetrators with lengths upwards of 8 cm and diameters of at least 1 cm [4]. But it is difficult to make ultrafine grain parts this large because of engineering constraints on workpiece dimensions in relevant processing routes.

In the present work, we use an alternate approach, evaluating the ballistic performance of an ultrafine grain tungsten alloy using small-caliber, spin-stabilized projectiles fired into concrete targets. Our results demonstrate the potential of sub-scale ballistic tests as a means of characterizing next-generation kinetic energy penetrator materials.

2. Materials and Methods

2.1. Penetrator Materials

We studied the ballistic performance of two different penetrator materials: a tungsten carbide cermet (WC-12Co, wt%) and a powder-processed, ultrafine-grained W alloy. A schematic of the cemented carbide penetrator is shown in Figure 1a. We used these conical nose cemented carbide rounds to calibrate the penetration equations described below. Quasi-static compression tests on specimens machined from these cemented carbide rounds gave an average failure stress of 3.8 GPa, with the samples failing by brittle fracture. The cemented carbide cores had a mass of 2.1 g and a specific gravity of 14.3 g/cm^3.

We also prepared sub-scale rounds from an ultrafine-grained W-Cr-Fe alloy whose chemistry and processing schedule were based on Ref. [2]. The material used in this study was prepared by 6 hours of attrition milling of elemental feedstock powders of W and Cr (99.95 pct W -100 mesh; 99+ pct Cr, -325 mesh) with an initial stoichiometry of W-10Cr, at%. Milling was performed under an Ar atmosphere using 200 g of powder, steel media, and a ball to powder ratio of 10:1.

The final chemistry of the as-milled powder was W-8Cr-4Fe, at% as measured by energy dispersive spectroscopy, where the Fe was introduced due to abrasion of the milling equipment. We consolidated the as-milled powder using a Dr. Sinter SPS-515S hot press, a graphite punch and die having a diameter of 24 mm, and the preferred consolidation parameters identified in Ref. [2]: a ramp rate of 100 K/min, a consolidation pressure of 100 MPa, a soak time of 1 min, and a soak temperature of 1200 °C. We then centerless ground samples electro-discharge machined from the center of these compacts into ogive nose rounds with the dimensions given in Figure 1b. We mounted in epoxy, cross-sectioned, and polished one of these W-8Cr-4Fe rounds using standard metallographic techniques, and characterized the microstructure of this cross-sectioned round using a JEOL 6610LV scanning electron microscope (SEM) operated at 20 kV and equipped with an energy dispersive spectrometer. We also measured this cross-sectioned round's Vickers microhardness using a LECO microhardness tester with a load of 100 gf and a hold time of 15 s. These microstructural investigations revealed that the W-8Cr-4Fe penetrators had a bimodal grain size distribution: approximately 85 vol% of the penetrator had a grain size of 200 nm, while the remaining material was coarse grained, with an average grain size exceeding 10 μm. As a result of their different grain sizes, the coarse- and fine-grained regions had different mechanical properties, with the fine grained regions having an average Vickers hardness of 10.8 GPa, more than double the Vickers hardness of the softer, coarse-grained regions. This difference is hardness is illustrated by the optical micrograph in Figure 2, which shows residual microhardness impressions in the coarse- and fine-grained regions. The coarse- and fine-grained regions also had different chemistries: the coarse-grained regions contained nominally pure W, while the fine grained regions contained W and the solute elements Fe and Cr, with an average stoichiometry of W-10Cr-6Fe as measured by energy dispersive spectroscopy.

These ultrafine grain tungsten penetrators had an average mass of 2.3 g, an average stereological porosity of 6%, and a specific gravity of 16.1 g/cm^3 as measured by the Archimedes method using high purity water as a reference liquid.

2.2. Ballistic Test Method

In the ballistic tests, we inserted the cemented carbide or the W-8Cr-4Fe core into a thin aluminum cup and copper jacket to increase the diameter to 5.56 mm. We then fired each assembly from a 5.56 mm diameter powder gun with a 1:7 twist and a 0.5 m long barrel, and varied the penetrators' incident velocities between 500 and 1100 m/s by varying the gun powder charge. We monitored the incident velocity as well as the pitch and yaw at impact using flash x-radiography [5]. Based on these flash x-ray measurements, we adjusted the muzzle-to-target distance between 3.3 and 3.9 m to minimize the pitch and yaw at impact, and only included tests with angles of incidence less than 4° in our analysis.

We fired all of the shots into targets prepared from the same batch of well-cured concrete. The concrete had a density of 2.2 g/cm^3 and contained aggregate with a volume-average, circular equivalent diameter of 2 mm. Cylindrical compression specimens with a 5 cm diameter and an aspect ratio of 2.5 that were cored from several targets had an average, unconfined compressive failure strength of 48 MPa. The concrete targets had cross-section dimensions of 20 by 20 cm and a thickness of 13 cm.

We measured the depth of penetration from the target's impact surface to the embedded penetrators' nose using static, post-test radiographs of the targets. The reported depths of penetration are the average of two measurements from radiographs taken at right angles to one another, which were generally in good agreement. The maximum depth of penetration that we

measured was roughly half the thickness of the target and there was no scabbing seen on the back face of the target after impact, so these targets could be approximated as semi-infinite.

2.3. Forrestal Analysis of Ballistic Results

To analyze the ballistic results, we used a framework developed by Forrestal and coworkers to describe rigid body penetration into concrete and geomaterials [4,6–17]. These researchers showed using penetrators with on-board accelerometers that the axial force on a projectile during impact can be described by the following relationships:

$$F = -cz \qquad z \leq 4R \tag{1a}$$

$$F = -\pi R^2(\sigma S + N\rho V^2) \qquad z > 4R \tag{1b}$$

where Eqns 1a and 1b describe the force equations during the cratering and tunneling phases of impact, respectively, and with *c*, *S*, and *N* constants that are defined below, *z* the instantaneous depth of penetration, *R* the radius of the penetrator, σ the unconfined compressive stress of the concrete target, ρ the density of the concrete, and *V* the instantaneous velocity of the penetrator [14,15,17].

The pre-factor *c* in Eqn 1a is a constant that depends on the incident velocity, V_S, as follows:

$$c = \frac{\pi R}{4}\left(\frac{S\sigma m + mV_S^2 N\rho}{m + 4\pi R^3 N\rho}\right) \tag{2}$$

where *m* is the penetrator's mass.

The constant *N* in Eqns 1b and 2 accounts for the shape of the penetrator's nose. For conical-nose penetrators, *N* is given by

$$N = \sin(\varphi)^2 \tag{3}$$

where φ is half the nose angle [18], and for ogive-nose penetrators, *N* is calculated using

$$N = \frac{8\psi - 1}{24\psi^2} \tag{4}$$

where $\psi = r/2R$ with r being the ogive radius [4]. Using Eqns 3 and 4, we calculated the N values of the cemented carbide and ultrafine grain tungsten cores to be 0.21 and 0.13, respectively.

The constant S in Eqns 1b and 2 is a fitting parameter that accounts for the strengthening of the concrete due to the hydrostatic compressive stress and high strain rates at the tip of the penetrator. Evaluating the equations of motion using Eqn 1a and 1b and the initial condition that $V = V_S$ at $z = 0$ gives the following relationship between the incident velocity and the depth of penetration

$$P = \frac{m}{2\pi R^2 \rho N} \log\left[\frac{S\sigma m + N\rho m V_s^2}{S\sigma(m + 4\pi R^3 N\rho)}\right] + 4R \qquad (5)$$

which can be fitted to experimental data to calibrate S.

3. Results and Discussion

Since Forrestal and coworkers validated their framework using penetrators with lengths ranging from 9 to 53 cm and diameters between 1.3 and 8 cm [4,14,15,17], we first demonstrated that their framework can also apply to small-caliber rounds using the cemented carbide penetrators. Figure 3a shows several radiographs of these cemented carbide penetrators embedded in the concrete targets. The dimensions of the cemented carbide penetrators in these radiographs are similar to those of the as-received rounds, suggesting rigid body penetration. This behavior was expected since the cemented carbide penetrators are two orders of magnitude stronger than the concrete targets.

The radiographs shown in Figure 2a also reveal distinct cratering and tunneling regions in the wake of the penetrator, with the average depth of the craters being 1 cm, or roughly twice the diameter of the penetrator. The morphology of this impact zone is consistent with Forrestal *et al.*'s previous reports of penetration into concrete [4,10,11,15].

In Figure 3b, we plotted the cemented carbide penetrators' incident velocities against their depths of penetration as well as a best fit to these results using Eqn 5 in order to test the validity of the

Forrestal framework. The close agreement between the ballistic results and the fit confirms that even small-caliber, rigid-body penetrators are well-described by the Forrestal equations. From the fit in Fig 3b, we found $S = 24$, which is twice that predicted by Forrestal et al. for concrete with a compressive strength of 48 MPa [4,11,13]. The reason for this discrepancy is the small ratio of the penetrator diameter to aggregate diameter in our work; the smaller this ratio, the larger S is for a given strength concrete, as noted by Beth [19] and others [14].

In light of these cemented carbide results, we next evaluated the penetration behavior of the W-8Cr-4Fe rounds using the Forrestal framework. Figure 4a shows radiographs of the W-8Cr-4Fe penetrators embedded in the concrete targets. Except for the 620 m/s shot, the tungsten alloy penetrators in these radiographs have dimensions similar to those of the as-received penetrators suggesting rigid body behavior. To further test for rigid body behavior, we plotted the W-8Cr-4Fe penetrator's depth of penetration as a function of incident velocity alongside the depth of penetration predicted by Eqn 5 in Figure 4b. Here we calculated the predicted depth of penetration using the S found from best fits to the cemented carbide data; best fits to the W-8Cr-4Fe data using Eqn 5 gave $S = 26$, which is just 10% larger. Besides a slight deviation between the predicted and measured depths of penetration at the highest incident velocity, which we can ascribe to the larger angle of incidence of that penetrator at impact (~2.5°), the agreement between the measured and predicted values suggest rigid body penetration, attesting to the high strength of this ultrafine grained alloy.

We can use the results from these sub-scale ballistic tests to compare different penetrator materials by estimating threshold velocities above which these small scale penetrators should start to transition from rigid body to eroding behavior. By normalizing Eqns 1a and 1b by the penetrator's

cross-sectional area, we can estimate the maximum nominal stress that the penetrators experience during impact as follows

$$\sigma_{\max} = \frac{S\sigma m + mV_s^2 N\rho}{m + 4\pi R^3 N\rho}. \quad (6)$$

Setting Eqn 6 equal to the yield strength of the penetrator material and solving for V_s gives a rough estimate of the threshold velocity, V_{max}, which differs from the Alekseevskii-Tate estimate of the threshold velocity by a factor of $\sqrt{2N}$ [3]. Note that our V_{max} represents an optimistic estimate since it assumes perfectly normal incidence, when in reality, oblique impact can generate bending moments that lead to fracture or plastic flow at lower incident velocities. With V_{max}, we can then calculate a kinetic energy density, $\rho_P(V_{max})^2$, where ρ_P is the density of the penetrator material, that can be used as a figure of merit for comparing different penetrator materials.

As an example of how to apply these concepts, we use them to compare our W-8Cr-4Fe material with high strength steel, the standard material used in concrete penetration. Our ultrafine grained W-8Cr-4Fe alloy has a dynamic compressive strength of 2.8 GPa as measured by Kolsky pressure bar experiments, so penetrators made from this alloy with the geometry shown in Figure 1b should start to yield at incident velocities of 2.2 km/s. By contrast, high strength steel penetrators with the same geometry and a yield strength of 1.5 GPa should start to yield at much lower incident velocities, around 1.2 km/s. Combined with the ~8 g/cc density of steel, these threshold velocities indicate that penetrators made from our ultrafine grained W-8Cr-4Fe alloy should be capable of delivering 7 times the kinetic energy of a high strength steel round before starting to transition from rigid body to eroding behavior.

4. Conclusions

Sub-scale ballistic tests into concrete have been performed using cemented carbide and ultrafine grained tungsten alloy penetrators. We found that the penetration behavior of these small-caliber

rounds was well-described by the Forrestal equations. After calibrating the fitting parameter in these equations, we were able to evaluate the performance of the ultrafine grained tungsten alloy penetrators and quantitatively demonstrate that they can behave as a rigid body penetrators over the range of velocities tested. These results together demonstrate the promise of this particular tungsten alloy as well as the potential of sub-scale ballistic testing as a tool for rapidly screening novel ballistic materials.

Acknowledgments

This work was supported by the U.S. Army Research Office under grant W911NF-14-1-0539 and through the Institute for Solider Nanotechnologies at MIT, and the US Defense Threat Reduction Agency under Grant No. HDTRA1-11-1-0062. ZCC also acknowledges support from the Department of Defense through the NDSEG fellowship program. The authors thank Dr. Deepak Kapoor of the Picatinny Arsenal and Steven Livers formerly of Boise State University for their assistance in preparing the ultrafine grain tungsten rounds; Dr. Lee Magness of the Army Research Laboratory for advising on the small-caliber testing geometry; and Prof. Emily Huskins for performing high strain rate compression tests on the ultrafine grain tungsten material.

References

[1] Q. Wei, H.T. Zhang, B.E. Schuster, K.T. Ramesh, R.Z. Valiev, L.J. Kecskes, et al., Microstructure and mechanical properties of super-strong nanocrystalline tungsten processed by high-pressure torsion, Acta Mater. 54 (2006) 4079–4089.

[2] Z.C. Cordero, E.L. Huskins, M. Park, S. Livers, M. Frary, B.E. Schuster, et al., Powder-Route Synthesis and Mechanical Testing of Ultrafine Grain Tungsten Alloys, Metall. Mater. Trans. A. 45 (2014) 3609–3618.

[3] Z. Rosenberg, E. Dekel, Terminal Ballistics, Springer Science & Business Media, 2012.

[4] M.J. Forrestal, B.S. Altman, J.D. Cargile, S.J. Hanchak, An empirical equation for penetration depth of ogive-nose projectiles into concrete targets, Int. J. Impact Eng. 15 (1994) 395–405.

[5] T.E. Ehlers, B.J. Guidos, D.W. Webb, Small-Caliber Projectile Target Impact Angle Determined from Close Proximity Radiographs, DTIC Document, 2006.

[6] M.J. Forrestal, Penetration into dry porous rock, Int. J. Solids Struct. 22 (1986) 1485–1500.
[7] V.K. Luk, M.J. Forrestal, Penetration into semi-infinite reinforced-concrete targets with spherical and ogival nose projectiles, Int. J. Impact Eng. 6 (1987) 291–301.
[8] M.J. Forrestal, V.K. Luk, H.A. Watts, Penetration of reinforced concrete with ogive-nose penetrators, Int. J. Solids Struct. 24 (1988) 77–87.
[9] M.J. Forrestal, V.K. Luk, Dynamic Spherical Cavity-Expansion in a Compressible Elastic-Plastic Solid, J. Appl. Mech. 55 (1988) 275–279.
[10] M.J. Forrestal, V.K. Luk, Penetration into soil targets, Int. J. Impact Eng. 12 (1992) 427–444.
[11] M.J. Forrestal, D.J. Frew, S.J. Hanchak, N.S. Brar, Penetration of grout and concrete targets with ogive-nose steel projectiles, Int. J. Impact Eng. 18 (1996) 465–476.
[12] M.J. Forrestal, D.Y. Tzou, A spherical cavity-expansion penetration model for concrete targets, Int. J. Solids Struct. 34 (1997) 4127–4146.
[13] D.J. Frew, S.J. Hanchak, M.L. Green, M.J. Forrestal, Penetration of concrete targets with ogive-nose steel rods, Int. J. Impact Eng. 21 (1998) 489–497.
[14] M.J. Forrestal, D.J. Frew, J.P. Hickerson, T.A. Rohwer, Penetration of concrete targets with deceleration-time measurements, Int. J. Impact Eng. 28 (2003) 479–497.
[15] D.J. Frew, M.J. Forrestal, J.D. Cargile, The effect of concrete target diameter on projectile deceleration and penetration depth, Int. J. Impact Eng. 32 (2006) 1584–1594.
[16] S.A. Silling, M.J. Forrestal, Mass loss from abrasion on ogive-nose steel projectiles that penetrate concrete targets, Int. J. Impact Eng. 34 (2007) 1814–1820.
[17] T.L. Warren, M.J. Forrestal, P.W. Randles, Evaluation of Large Amplitude Deceleration Data from Projectile Penetration into Concrete Targets, Exp. Mech. 54 (2013) 241–253.
[18] M.J. Forrestal, K. Okajima, V.K. Luk, Penetration of 6061-T651 aluminum targets with rigid long rods, J. Appl. Mech. 55 (1988) 755–760.
[19] R.A. Beth, Concrete Penetration, Natl Defense Research Committee Report A-319, 1946.

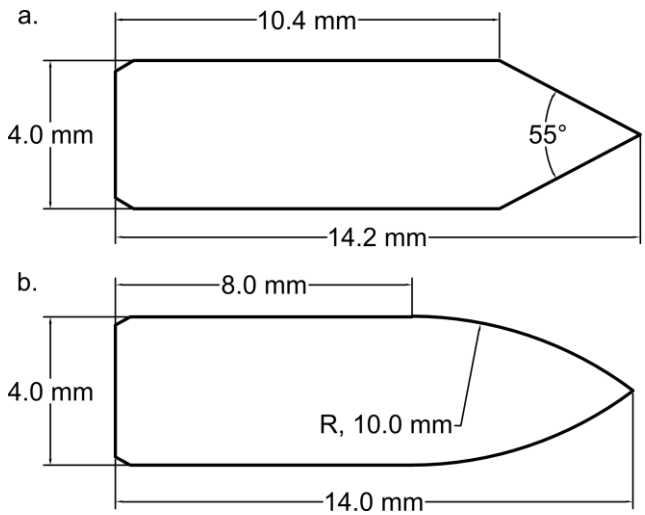

Figure 1 – Schematics of the a) cemented carbide and b) W-8Cr-4Fe penetrators.

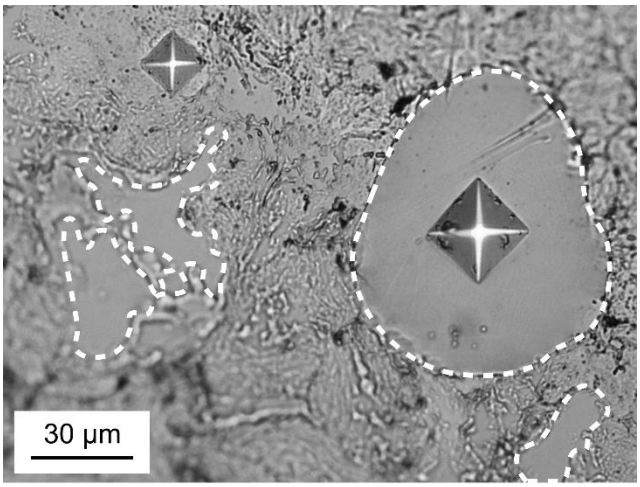

Figure 2 – Optical micrograph of Vickers microhardness impressions in the coarse- and fine-grained regions. The softer, coarse-grained regions are indicated by the dashed white lines.

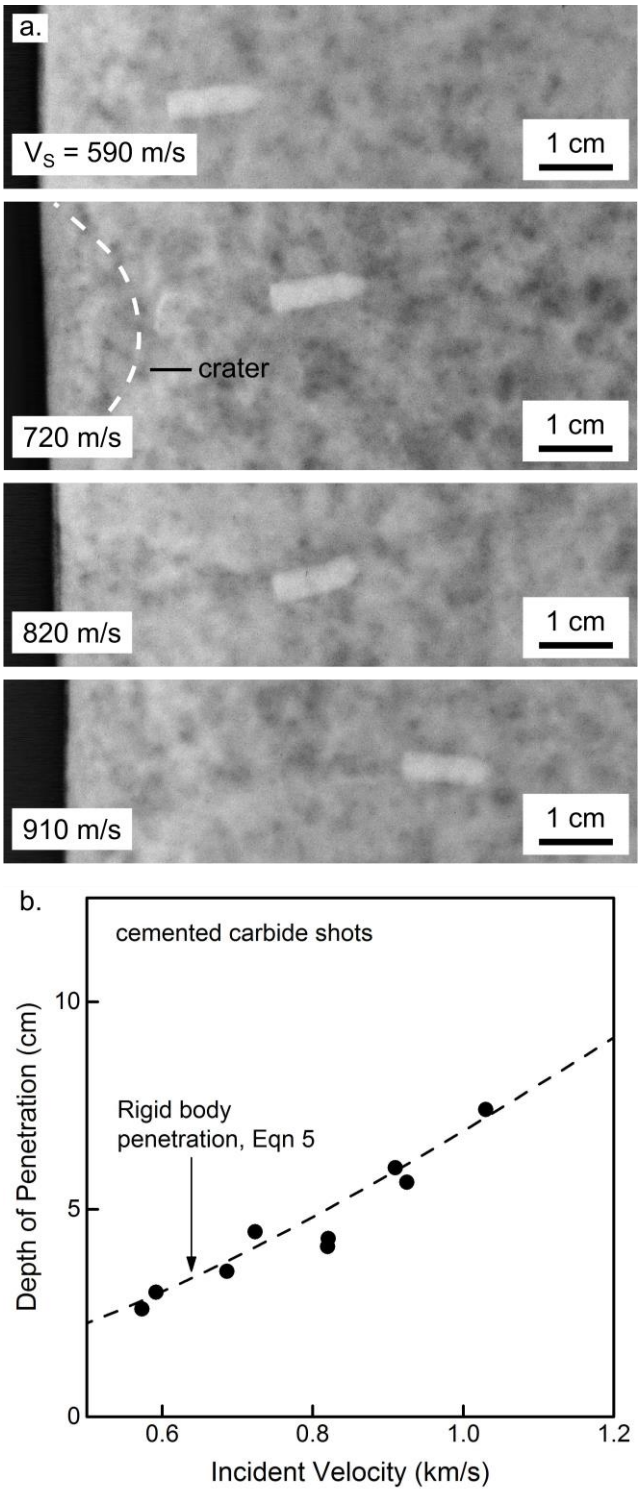

Figure 3 – a) Radiographs of cemented carbide rounds that struck the targets at the velocities indicated. The crater region is highlighted in the radiograph of the penetrator that had an incident velocity of 720 m/s. b) Cemented carbide rounds' depths of penetration as a function of incident velocity. The dashed line is the best fit to the data using Eqn 5.

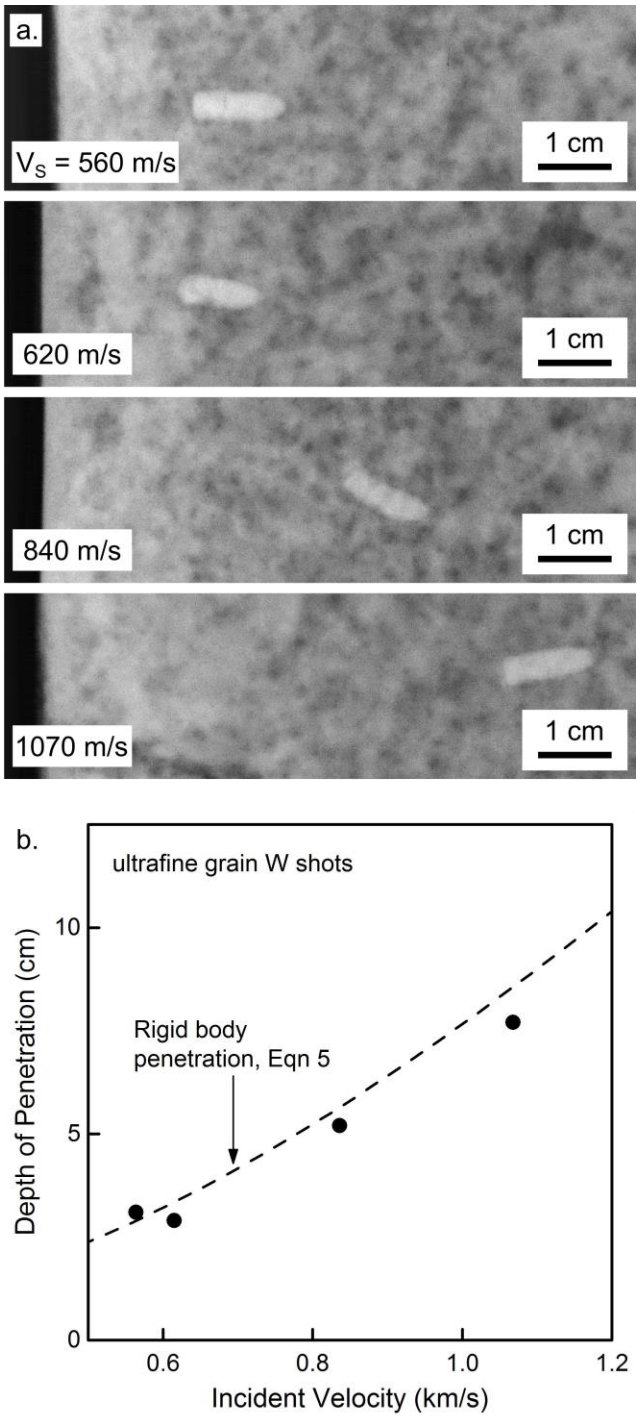

Figure 4 – a) Radiographs of W-8Cr-4Fe rounds embedded in the concrete targets. b) Depth of penetration of the W-8Cr-4Fe penetrators as a function of incident velocity. The rigid body depth of penetration predicted using Eqn 5 is shown as well.